

# Inversion Potentials for Meson–Nucleon and Meson–Meson Interactions\*

M. Sander and H.V. von Geramb

*Theoretische Kernphysik, Universität Hamburg,  
Luruper Chaussee 149, D-22761 Hamburg, Germany*

## Abstract

Two-body interactions of elementary particles are useful in particle and nuclear physics to describe qualitatively and quantitatively few- and many-body systems. We are extending for this purpose the quantum inversion approach for systems consisting of nucleons and mesons. From the wide range of experimentally studied two-body systems we concentrate here on  $\pi N$ ,  $\pi\pi$ ,  $K^+N$ ,  $K\pi$  and  $K\bar{K}$ . As input we require results of phase shift analyses. Quantum inversion Gelfand–Levitan and Marchenko single and coupled channel algorithms are used for Schrödinger type wave equations in partial wave decomposition. The motivation of this study comes from our two approaches: to generate and investigate potentials directly from data by means of inversion and alternatively use linear and nonlinear boson exchange models. The interesting results of inversion are coordinate space informations about radial ranges, strengths, long distance behaviors, resonance characteristics, threshold effects, scattering lengths and bound state properties.

---

\*Contribution to the International Conference on Inverse and Algebraic Scattering Theory, Lake Balaton '96

## I. INTRODUCTION

It is a paradigm of particle and nuclear physics to describe complex many-body systems in terms of two-body interactions or two-body  $t$ -matrices. The formulation of a two-body interaction is therefore a central goal for generations of physicists, both of the experimental and theoretical community. Roughly speaking, we separate these efforts of finding two-body interactions into groups which orient themselves very closely on data, whereas the other extreme follows a fundamental approach. In another contribution to this conference we have dwelled upon the need to follow both approaches [1].

Encouraged by the tremendous success of the inverse scattering method for fixed angular momentum in application to nucleon-nucleon interactions we extend our study in this contribution to meson-nucleon and meson-meson systems in the framework of the Gelfand-Levitan and Marchenko theory. A comprehensive description of our mathematical and numerical framework can be found elsewhere [2,3] and we shall concentrate here solely on the presentation and interpretation of results which are a small fraction of all results contained in the thesis [4]. In particular we study  $\pi N$ ,  $\pi\pi$ ,  $K^+N$ ,  $K\pi$  and  $K\bar{K}$  scattering. As experimental input for the inversion algorithms we used phase shift analyses of Arndt et al. for  $\pi N$  [5] and  $K^+N$  [6], of Froggatt et al. for  $\pi\pi$  [7] and of Estabrooks et al. for  $K\pi$  [8]. We limit ourselves to subinelastic and subreaction threshold data. An effective range parameterization is used for the  $K\bar{K}$  system [9]. A critical and comprehensive assessment of the data can be found in [4].

For the two-body system the relativistic Schrödinger equation

$$-f_\ell''(k, r) + \left( \frac{\ell(\ell+1)}{r^2} + 2\mu(s)V_\ell(r) \right) f_\ell(k, r) = k^2 f_\ell(k, r) \quad (1)$$

is assumed to be valid. The CM parameters are given by

$$k^2 = \frac{m_2^2(T_{Lab}^2 + 2m_1T_{Lab})}{(m_1 + m_2)^2 + 2m_2T_{Lab}}. \quad (2)$$

or

$$k^2 = \left( \frac{s - m_1^2 - m_2^2}{2\sqrt{s}} \right)^2 - \frac{m_1^2 m_2^2}{s} \quad (3)$$

with

$$s = M_{12}^2 = \left( \sqrt{k^2 + m_1^2} + \sqrt{k^2 + m_2^2} \right)^2 = (m_1 + m_2)^2 + 2m_2 T_{Lab}, \quad (4)$$

$m_1, m_2$  are the masses of the projectile and the target and  $T_{Lab}$  is the kinetic energy in the laboratory. The experimental data are given either as a function of  $T_{Lab}$  or the Mandelstam variable  $s$ . As reduced mass  $\mu(s)$  we use either the non-relativistic reduced mass

$$\mu = \frac{m_1 m_2}{m_1 + m_2} \quad (5)$$

or the reduced energies [10]

$$\mu(s) = \frac{1}{2} \frac{dk^2(s)}{d\sqrt{s}} = \frac{1}{2} \frac{s^2 - (m_1^2 - m_2^2)^2}{2s^{3/2}}. \quad (6)$$

This expression (6) is generally approximated by the low-energy limit or the conventional non-relativistic reduced mass. Any of these options is to be motivated by the application of the interaction potentials in other contexts. Depending on the choice of the reduced mass, we obtain different inversion potentials. The potential is in any case local and energy independent but dependent on the channel quantum numbers ( $\ell S J T$ ). Our numerical algorithm guarantees that insertion of the potential in eqn. (1) reproduces the input phase shifts  $\delta(k)$  better than  $0.02^\circ$ .

The simplicity of our potential operator may be surprising in view of the non-locality implied by results from meson exchange models. It is also our opinion that the actual potential should be non-local, but we understand that the inversion potential represents a local equivalent yielding the same on-shell two-body t-matrix for the full operator. The local potential permits to compute off-shell t-matrices with a Lippmann-Schwinger equation with the implication that a non-local potential may yield a different off-shell continuation than a local potential. This difference in the off-shell domain can become important in few- and many-body systems or in the interaction regions of two-body wave-functions.

For nucleon–nucleon systems we have put much effort in attempts to clarify this point and find no evidence for differences in observables [1,4]. This is a very surprising result and it is the purpose of this study to initiate a comparison of strictly equivalent local on–shell potentials with their non–local counterparts in the realm of meson–nucleon and meson–meson interactions.

## II. $\pi N$ SCATTERING

Partial wave phase shifts of the  $\pi N$  system are determined by an analysis of elastic and charge exchange scattering  $\pi^+p \rightarrow \pi^+p$ ,  $\pi^-p \rightarrow \pi^-p$  and  $\pi^-p \rightarrow \pi^0n$ . They form a complete set of observables entering a partial wave analysis with isospin  $T = \frac{1}{2}$  and  $\frac{3}{2}$  [5]. The notation for the isospin and angular momentum channels is  $\ell_{2T,2S}$ . We used the SM95 analysis of Arndt et al. for channels  $\ell \leq 3$  [4,5].

### A. $\pi N$ p–Wave Resonances

The most prominent resonances are the  $\Delta(1232)$  in the  $P_{33}$  and the  $N(1440)$  Roper resonance in the  $P_{11}$  channels. The phase shifts for these resonances are shown in the left part of Fig. 1. We factorize the S–matrix into a *resonant* and a *non–resonant* part  $S(k) = S_r(k)S_p(k)$ . For the resonant part we use a resonance and an auxiliary pole parameterization [11]

$$S_r(k) = \frac{(k + k_r)(k - k_r^*)(k + k_h)(k - k_h^*)}{(k - k_r)(k + k_r^*)(k - k_h)(k + k_h^*)}, \quad (7)$$

which contains the right amount of zeros and poles for a decomposition into Jost functions. The rest  $S_p(k)$  of the S–matrix is parameterized in our usual parameterization scheme for  $\delta_p(k)$  in connection with the symmetric Padé approximant for the exponential function [3].

In Table I are summarized the relevant parameters for this decomposition using SM95 [5]. As shown in Fig. 1 (left) this reproduces the input phase shifts very well for  $T_\pi \leq 500$  MeV. In Fig. 1 (right) we show the inversion potential for the  $P_{33}$  channel with a repulsive well,

enabling tunneling for the pion–nucleon system, with a very strong short range attraction, which yields the  $\Delta(1232)$  quasi bound state. The long range part of this potential, not visible in Fig. 1, behaves like a Yukawa tail with a strength  $Y = 650.0$  [MeVfm] and  $\mu = 1.77$  [fm $^{-1}$ ], see also section V. The relative distance of the centers of mass in the strong attractive region is unexpectedly small,  $r \leq 0.25$  fm. In view of the large radii of the charge form factor of the pion and the nucleon, approximately 0.54 fm for the pion and 0.7 fm for the nucleon, this relative distance implies more than 90% overlap of the intrinsic structures before the strong attractive potential simulates a phase transition of the pion–nucleon quark content into the 3–quark content of the  $\Delta$ . Ultimately such explanation must be confirmed by QCD calculations. We decline and warn from a far reaching interpretation of this potential with its strength and radial dimensions.

### B. $\pi N$ Scattering Lengths and $\pi NN$ Coupling Constants

From the  $\pi N$  potentials in the  $T = \frac{1}{2}, \frac{3}{2}$  s–channels we find the scattering lengths  $a_1 = 0.178$  [m $_{\pi}^{-1}$ ],  $a_3 = -0.088$  [m $_{\pi}^{-1}$ ]. For a comparison with several other predictions see Table II. These results may be used in the Goldberger–Miyazawa–Oehme sum rule [16]

$$\frac{f_{\pi NN}^2}{4\pi} = \frac{(m_{\pi}^2 - \mu^2)(m_N + m_{\pi})}{6m_N m_{\pi}}(a_1 - a_3) - \frac{m_{\pi}^2 - \mu^2}{8\pi^2} \int_0^{\infty} \frac{\sigma_{\pi^- p} - \sigma_{\pi^+ p}}{\sqrt{q^2 + m_{\pi}^2}} dq \quad (8)$$

to obtain a model independent estimate for the  $\pi NN$  coupling constant. Using the simplified form of this sum rule [17]

$$\frac{f_{\pi NN}^2}{4\pi} = 0.19m_{\pi}(a_1 - a_3) - (0.025 \text{ mb}^{-1})\mathcal{J}, \quad (9)$$

where the integral

$$\mathcal{J} = \frac{1}{4\pi^2} \int_0^{\infty} \frac{\sigma_{\pi^- p} - \sigma_{\pi^+ p}}{\sqrt{q^2 + m_{\pi}^2}} dq \quad (10)$$

has the VPI value  $\mathcal{J} = -1.041$  mb, we find

$$\frac{f_{\pi NN}^2}{4\pi} = 0.0766, \quad \text{or} \quad \frac{g_{\pi NN}^2}{4\pi} = 13.84, \quad (11)$$

which is fully consistent with the value of  $13.75 \pm 0.15$  given in [5].

### C. $\pi^-p$ Atoms

The Coulomb attraction between  $\pi^-$  and  $p$  causes a bound system called pionic hydrogen  $A_{\pi p}$ . Additionally, the hadronic interaction between the two constituents distorts the short range interaction and changes the pure Coulomb spectrum. Decay channels  $\pi^-p \rightarrow \pi^0n$  and  $\pi^-p \rightarrow \gamma n$  allow a rapid decay.

The hadronic shift of the  $3p \rightarrow 1s$  transition and the total  $1s$  width has recently been measured at PSI [13]. To analyze this experiment we use quantum inversion for the determination of the hadronic potentials. Inelasticities, Coulomb and other isospin breaking effects are supposed to be not included in the SM95 phase shift analysis [5]. Using the  $S_{11}$  and  $S_{31}$  phase shifts shown in Fig. 2, we obtain the hadronic potentials  $V_{11}(r)$  and  $V_{31}(r)$ , Fig. 3 (left). The inversion algorithm uses only the nonrelativistic reduced mass  $\mu = 121.50$  MeV based upon the  $\pi^\pm$  and  $p$  masses, consistently with the phase shift analysis.

In the next step we apply a rotation of these potentials in isospin space from good isospin states into particle eigenstates. This yields the potential matrix  $V^{ij}(r)$  of the coupled radial Schrödinger equation

$$f_i'' + k_i^2 f_i = \sum_{j=1}^2 2\mu_i V^{ij} f_j, \quad i = 1(2) \text{ for } \pi^-p (\pi^0n) \quad (12)$$

for the  $\pi^-p \leftrightarrow \pi^0n$  system. The potential matrix contains the isospin rotation coefficients and the Coulomb attraction

$$V^{11} = V^{\pi^-p} = \frac{2}{3}V_{11} + \frac{1}{3}V_{31} - \frac{e^2}{r}, \quad (13)$$

$$V^{12} = V^{21} = -\frac{\sqrt{2}}{3}(V_{11} - V_{31}), \quad (14)$$

$$V^{22} = V^{\pi^0n} = \frac{2}{3}V_{31} + \frac{1}{3}V_{11}. \quad (15)$$

The hadronic part of this matrix is shown on the right side of Fig. 3. The reduced masses we used are  $\mu_1 = 121.50$  MeV and  $\mu_2 = 118.02$  MeV. In Table III we signal this choice with the parameter  $x = -1$ . This mass difference introduces an additional isospin breaking effect. Since this issue is of central importance for the pion-pion system in the next section we

investigate this point in further details also here and distinguish the alternative calculation with  $\mu_1 = \mu_2 = 121.50$  MeV and  $x = +1$ . Generally it is assumed that charge and mass isospin-breaking effects should have a small impact on the lifetime and width of  $A_{\pi p}$  or the eigenchannel phase shifts.

The bound states of the  $\pi^-p$  system can be found as resonances in the energetically open  $\pi^0n$  channel, showing a partial width  $\Gamma_{ns}^{\pi^-p \rightarrow \pi^0n}$  deduced from the elastic cross section

$$\sigma(\pi^0n \rightarrow \pi^0n) = \frac{\pi}{k_2^2} |1 - S_{22}|^2. \quad (16)$$

Results for the ground state are given in Table III. To account for the full experimental width one has to correct the partial width with the Panofsky ratio  $P = 1.546 \pm 0.009$  [13]

$$\Gamma_{ns} = \left(1 + \frac{1}{P}\right) \Gamma_{ns}^{\pi^-p \rightarrow \pi^0n}. \quad (17)$$

To show the effect of isospin breaking caused by different reduced masses in channel 1 and 2, we repeated this calculation with  $\mu_2(\pi^0n)$  set equal to  $\mu_1(\pi^-p)$ . These results are also included in Table III with  $x = +1$ . Furthermore we have accounted for the  $\gamma n$  decay by the introduction of a phenomenologic imaginary Gaussian potential  $W(r) = W_{11} = -9 \exp(-4r^2)$  in eqn. (12), where we replace  $V_{11} \rightarrow V_{11} + iW_{11}$ . The point Coulomb potential is replaced by double folded Gaussian charge distributions for the pion and nucleon

$$\frac{e^2}{r} \rightarrow \frac{e^2 \Phi(1.13 r)}{r}.$$

All results are shown in Table III. They agree well with the experimental values, and the small isospin breaking effects from the mass difference confirm our assumption and establish an excellent support of the inversion approach.

### III. $\pi\pi$ SCATTERING

$\pi\pi$  phase shifts come from the analysis of final state interactions in  $\pi N \rightarrow \pi\pi N$  systems or the  $K_{e4}$ -decay  $K^- \rightarrow \pi^+\pi^-e\bar{\nu}$ . Here we use results of the CERN-Munich experiment [7]  $\pi^-p \rightarrow \pi^+\pi^-n$  for all channels with  $\ell \leq 3$ . The scattering is purely elastic up to

$M_{\pi\pi} = 987.3$  MeV where a coupling  $\pi^+\pi^- \leftrightarrow K\bar{K}$  becomes dominant. In addition to the experimental data of Froggatt et al. [7] we use data from meson exchange models [18] and chiral perturbation theory  $\chi$ Pt [19]. Notation for the isospin and angular momentum channels uses  $\delta_\ell^T$  or  $V_\ell^T$ . The inversion results are shown in Fig. 4.

Similar to the  $\pi^-p$  system there exists pionium  $A_{\pi\pi}$  which is formed by  $\pi^-\pi^+$  Coulomb attraction and decays by charge exchange into the open  $\pi^0\pi^0$  channel. The coupled channel system is equivalent to eqn. (12) replacing  $p \rightarrow \pi^+$  and  $n \rightarrow \pi^0$ . We assume the same approach and rotate the good isospin potentials into particle states [22] which reduces to the same form as given by eqn. (13) – (15), simply replace  $V_{11} \rightarrow V_0^0$  and  $V_{31} \rightarrow V_0^2$ . Phase shift analyses and inversion use a single mass  $\mu = m_{\pi^+}/2$  without Coulomb effects. This assumption guarantees good isospin  $T = 0$  and  $2$ . With the purpose to display uncertainties in the phase shifts we used three sources and distinguish a set of three potentials for  $V_0^0$  and  $V_0^2$  respectively. They are shown in Fig. 4 (right), of which the  $V_0^0$  potential is of particular interest. Similar to the  $\pi N P_{33}$  channel potential we find here a potential barrier and a very strong short range attraction. Such potential may be able to support a potential resonance similar to the  $\Delta$ -resonance in the  $\pi N P_{33}$  channel, but here in the  $\ell = 0, T = 0$  channel the resonance width is expected larger than for  $\ell = 1$  since the resonance conditions are more delicate due to the centrifugal barrier. The radial dimensions and potential strengths are quite comparable. It is obvious to ask if the implied great width resonance supported by this potential can be identified with the isoscalar  $\sigma$  meson which OBE potential require and which is of general interest [23,24,25,26]. It is intended to study this resonance in more details by our OSBEP approach and use also other experimental information. A first glance on this investigation is given by simply using different reduced masses in eqn. (12). This changes effectively the strength of  $V_0^0$  within a few % but causes a dramatic change of the eigenchannel phase shifts which can be identified with the  $T = 0$  isospin state. In Fig. 5 we show three cases of different choices of  $\mu_i$ . Fig. 5 (top left)  $\mu_1 = \mu_2 = m_{\pi^+}/2$  without Coulomb potential. This confirms the original input phase shifts used for the inversion. (top right)  $\mu_1 = m_{\pi^+}/2, \mu_2 = m_{\pi^0}/2$  which are the correct reduced masses in the nonrelativistic



limit. As expected, the eigenchannel phase  $\delta_0^2$  remains unchanged, whereas  $\delta_0^0$  is now far off the data. (bottom)  $\mu_1 = \mu_2 = m_{\pi^0}/2$  is a further step, and we observe little change for  $\delta_0^2$  but a dramatic effect for  $\delta_0^0$ . This investigation is supposed to show that the strength of the potential enters very sensitively and changes the  $\delta_0^0$  phase in a wide range quite untypical for a resonance. The effects upon the lifetime of pionium has already been studied and we observe a dramatic change of lifetime compared between what is given in Table IV and [22]. This change requires a deeper understanding since the hypothetical  $\sigma$ -meson is producing the medium-range  $NN$  attraction. Medium effects of this resonance should be of particular importance and we are presently studying this aspect in microscopic optical potentials for nucleon-nucleus scattering.

#### IV. $K^+N$ , $K\pi$ AND $K\bar{K}$ SCATTERING

##### A. $K^+N$ Scattering

Kaons introduce strangeness into the inversion algorithm where the configurations  $K^+N, K^0N$  with  $S = +1$  and  $K^-N, \bar{K}^0N$  with  $S = -1$  are allowed in  $KN$  scattering. The  $S = -1$  channels show strong resonance effects whereas the the  $S = +1$  channels are smooth. Phase shift analyses are restricted by Arndt in SP92 [6] to the  $K^+N$  system. In Fig. 6 we show the result for  $\ell = 3$ , the nomenclature used is  $\ell_{T,2J}$ ,  $J = \ell \pm \frac{1}{2}$ . The results show little structure in the radial dependencies. Undoubtedly the range of the potential is longer than for the  $\pi N$  system. The long range part of the interaction is discussed in section V. We calculated  $K^+N$  s-wave scattering lengths from inversion potentials and compare them with predictions of the phase shift analysis and models. They are summarized in Table V. Predictions from meson exchange models [27] agree either with the  $T = 0$  or 1 scattering lengths.

## B. $K\pi$ scattering

Suitable informations for  $K\pi$  scattering come from final state interaction analyses of the reactions  $K^\pm p \rightarrow K^\pm \pi^+ n$ , and  $K^\pm p \rightarrow K^\pm \pi^- \Delta^{++}$ . The notation for channel identification is  $\delta_\ell^{2T}$ , where  $T = \frac{1}{2}$  or  $\frac{3}{2}$ . Well known resonances in this system are  $K^*(892)$  and  $K_0^*(1430)$ . The phase shift analysis starts at  $M_{K\pi} = 0.73$  GeV and remains elastic up to 1.3 GeV [8]. There is a gap between threshold,  $M_{K\pi} = 0.63$  GeV, and the first data points. We bridged this gap with a smooth extrapolation with  $\lim_{k \rightarrow 0} \delta_\ell^{2T}(k) = \mathcal{O}(k^{2\ell+1})$  [4].

Our scattering lengths, see Table VI, agree well with estimates from dispersion relations ( $0.22 \geq a_0^1 \geq 0.045$ ,  $-0.10 \geq a_0^3 \geq -0.165$ ) [31] and the experimental values [8], but they are 1.4 to 3 times larger than predictions from various models. To solve this puzzle, more data between the  $K\pi$  threshold and  $M_{K\pi} = 730$  MeV are needed.

## C. $K\bar{K}$ Scattering

There exist no phase shift analyses for this system, and we have to rely upon an effective range expansion by Kaminski and Lesniak [9]. Their expansion may be disputed since they neglect inelasticities. This describes briefly the experimental situation with the implication that our analysis represents only some qualitative features.

We are using two sets of parameters from [9] in the effective range expansion

$$k \cot \delta_K(k) = \frac{1}{\text{Re } a_K} + \frac{1}{2} R_K k^2 + V_K k^4 \quad (18)$$

whose values are given in Table VII. The phase shifts  $\delta_0(M_{KK})$  from this parameterization are shown in Fig. 7, together with the inversion potentials which reproduce the effective range expansion with high precision. There exists a claim from lattice QCD that the short range attractive interaction has an explanation in a non-vanishing propagator structure [32].

## V. LONG RANGE BEHAVIORS

In the display of inversion potentials we restricted ourselves to the big effects at distances between 0–2 fm and emphasized the short range domain. Actually, the most reliable information is the long range part of the potentials which can be parameterized in terms of a Yukawa potential with a range parameter given by the Compton wave length of an exchanged particle. For the pion–nucleon system we have also dwelled upon the coupling constant. In Table VIII are summarized the long range Yukawa parameters  $V(r) = Y e^{-\mu r} / r$  which we extracted from our inversion potentials in the  $\ell = 0$  channels. We find that the exchanged masses in  $pp$ ,  $K\bar{K}$  and  $K^+N$  may be interpreted as one–pion, two–pion and one– $\sigma_1$  exchange respectively. From the microscopic point of view, the propagators of a dominant pseudoscalar or scalar  $s$ –channel exchange transform into a Yukawa–like potential tail. In  $\pi N$ ,  $\pi K$  and  $\pi\pi$  scattering this interpretation is not valid, since here  $s$ – and  $t$ –channel graphs contribute and thus a transformation into coordinate space does not lead to a Yukawa with a physical mass of an exchange particle. A more detailed discussion of this table and its implications can be found in [4].

## VI. SUMMARY AND CONCLUSIONS

With this contribution we show that the rich sources of phase shift analyses for general hadronic systems can successfully be used to obtain a qualitative and sometimes quantitative understanding of the interaction in terms of a simple local potential. The ranges and strengths of these potentials are often determined by the masses of the scattered particles and the spin–isospin dependence of the partial waves. This dependence can often be understood in terms of a boson exchange picture and ultimately may be related to the underlying QCD dynamics. The latter aspect is most obvious in the  $p$ –wave resonances of the  $\pi N$  system. With this first attempt of using quantum inversion to study the realm of hadronic interactions we establish encouragement to look for alternative equations of motion which

should account better for the relativistic kinematics which is definitely important for the lighter hadronic systems or any extension towards higher energy. Various relativistic wave equations have been studied and applied in recent years when treating hadrons with quarks as their constituents.

### **ACKNOWLEDGMENTS**

Supported in part by Forschungszentrum Jülich, COSY Collaboration 41126865.

## REFERENCES

- [1] L. Jäde, M. Sander and H.V. von Geramb, *these conference proceedings* and nucl-th/9609054
- [2] K. Chadan and P.C. Sabatier, *Inverse Problems in Quantum Scattering Theory, 2nd. Edition*, Springer, Berlin (1989)
- [3] H.V. von Geramb and H. Kohlhoff, in: H.V. von Geramb (ed.), *Quantum Inversion Theory and Applications*, Lecture Notes in Physics 427, Springer, Berlin (1994); H. Kohlhoff and H.V. von Geramb, *ibid.*
- [4] M. Sander, PhD Thesis (in german), University of Hamburg (1996)
- [5] R.A. Arndt, I.I. Strakowsky, R.L. Workman and M.M. Pavan, Phys. Rev. **C52**, 2120 (1995)
- [6] J. S. Hyslop, R. A. Arndt, L. D. Roper and R. L. Workman, Phys. Rev. **D46**, 961 (1992)
- [7] C.D. Froggatt and J. L. Petersen, Nucl. Phys. **B129**, 89 (1977)
- [8] P. Estabrooks et al., Nucl. Phys. **B133**, 490 (1978)
- [9] R. Kaminski and L. Lesniak, Phys. Rev. **C51**, 2264 (1995)
- [10] B.L.G. Bakker and P.J. Mulders, Adv. Nucl. Phys. **17**, 1 (1986)
- [11] V.I. Kukulin, V.M. Krasnopol'sky und J. Horáček, *Theory of Resonances*, Academia, Prague (1989)
- [12] R. Koch and E. Pietarinen, Nucl. Phys. **A336**, 331 (1980)
- [13] D. Sigg et al., Phys. Rev. Lett. **75**, 3245 (1995)
- [14] B.C. Pearce and B.K. Jennings, Nucl. Phys. **A528**, 655 (1991)
- [15] C. Schütz, J.W. Durso, K. Holinde and J. Speth, Phys. Rev. **C49**, 2671 (1994)

- [16] M.L. Goldberger, H. Miyazawa and R. Oehme, Phys. Rev. **99**, 986 (1955)
- [17] R.L. Workman, R.A. Arndt and M.M. Pavan, Phys. Rev. Lett. **68**, 1653 (1992)
- [18] D. Lohse, J.W. Durso, K. Holinde and J. Speth, Nucl. Phys. **A516**, 513 (1990)
- [19] J. Gasser and H. Leutwyler, Phys. Lett. **125B**, 325 (1983)
- [20] L.G. Afanasyev et al., Phys. Lett. **B308**, 200 (1993); L.G. Afanasyev et al., Phys. Lett. **B338**, 478 (1994)
- [21] G.V. Efimov, M.A. Ivanov and V.E. Lyubovitskii, Sov. J. Nucl. Phys. **44**, 296 (1986)
- [22] M. Sander, C. Kuhrts and H.V. von Geramb, Phys. Rev. **C53**, R2610 (1996)
- [23] N.A. Törnqvist and M. Roos, Phys. Rev. Lett. **76**, 1575 (1996)
- [24] N. Isgur and J. Speth, Phys. Rev. Lett. **77**, 2332 (1996); N.A. Törnqvist and M. Roos, *ibid.*, 2333 (1996)
- [25] M. Harada, F. Sannino and J. Schechter, Los Alamos e-print archive hep-ph/9609428; N.A. Törnqvist and M. Roos, *ibid.* hep-ph/9610527
- [26] S. Ishida et al., Los Alamos e-print archive hep-ph/9610359
- [27] R. Büttgen, K. Holinde, A. Müller-Groeling, J. Speth and P. Wyborny, Nucl. Phys. **A506**, 586 (1990)
- [28] V. Bernard, N. Kaiser and U.-G. Meissner, Phys. Rev. **D43**, R2757 (1991)
- [29] T. Barnes, E.S. Swanson and J. Weinstein, Phys. Rev. **D46**, 4868 (1992)
- [30] Z. Li, M. Guidry, T. Barnes and E.S. Swanson, Bulletin Board hep-ph/9401326
- [31] A. Karabarounis and G. Shaw, J. Phys. **G6**, 583 (1980)
- [32] H. R. Fiebig, H. Markum, A. Mihály, K. Rabitsch and C. Starkjohann, Nucl. Phys. B (Proc. Suppl.) **47**, 394 (1996)

TABLES

TABLE I.  $\pi N$  resonance parameters used in the inversion scheme.

$\pi N$ channel	$\text{Re}(k_r)$ [ $\text{fm}^{-1}$ ]	$\text{Im}(k_r)$ [ $\text{fm}^{-1}$ ]	Mass [MeV]	Width [MeV]	Name
$P_{11}$	1.8200	-0.6200	1381	159	N(1440)
$P_{33}$	1.0665	-0.2440	1212	102	$\Delta(1232)$
$D_{13}$	2.2900	-0.1050	1514	93	N(1520)
$F_{15}$	2.8520	-0.1230	1674	72	N(1680)

TABLE II.  $\pi N$   $s$ -wave scattering lengths from several models and experimental analyses together with predictions for the  $\pi NN$  coupling constant obtained from the GMO sum rule.

Model	$a_1$ [ $m_\pi^{-1}$ ]	$a_3$ [ $m_\pi^{-1}$ ]	$f_{\pi NN}^2/4\pi$	Ref.
SM95 Inversion	0.178	-0.088	0.0766	
KH80	0.173	-0.101	0.079	[12]
$\pi^- p$ 1s state	0.185	-0.104	0.081	[13]
Pearce et al.	0.151	-0.092	0.072	[14]
Schütz et al.	0.169	-0.085	0.074	[15]

TABLE III. Hadronic shift of the  $1s$  level, with respect to the pure Coulombic reference energy  $E_{1s}^C = 3234.9408$  [eV], and partial widths  $\Gamma_{1s}^{\pi^- p \rightarrow \pi^0 n}$ . These partial widths have to be multiplied with 1.647 to account for the Panofsky ratio to obtain the total widths. This yields a typical value  $\sim 0.862$  [eV] to be compared with the experimental value  $\Gamma_{1s} = 0.97 \pm 0.10 \pm 0.05$  [eV]. The strength of the imaginary part in the last entry  $W_{11}$  is adjusted to reproduce the experimental value.

x	Point Charge Coulomb		Gaussian Charge Coulomb		
	Shift [eV]	FWHM [eV]	Shift [eV]	FWHM [eV]	
-1	-7.13259	0.5187	-7.01055	0.5144	
+1	-7.29821	0.5250	-7.16746	0.5230	
$\mu(s)$	-7.26334	0.5317	-7.13259	0.5266	
	Shift = $-7.127 \pm 0.046$ [eV], $\Gamma_{1s}^{\pi^0 n} = 0.590$ [eV]				Sigg [13]
-1	-7.23259	0.9763	-7.12387	0.9763	$V_{11} + iW_{11}$
	Shift = $-7.127 \pm 0.028 \pm 0.036$ [eV], $\Gamma_{1s} = 0.97 \pm 0.10 \pm 0.05$ [eV]				Sigg [13]

TABLE IV.  $A_{\pi\pi}$  properties from inversion potentials. The Point Coulomb ground state reference energy  $E_{1s}^C = 1.85807248$  [keV]. ( $x=+1$ )  $\equiv \mu_1 = \mu_2 = m_{\pi^+}/2$ .

x	$E_{1s}$ [keV]	Shift [eV]	$\tau$ [ $10^{-15}$ sec]	FWHM [eV]	Reference
+1	1.8638814	-5.809	1.97	0.3481	Froggatt
$\mu(s)$	1.8636070	-5.538	2.05	0.3337	Froggatt
+1	1.8635114	-5.439	1.89	0.3627	Lohse
$\mu(s)$	1.8632880	-5.216	2.03	0.3385	Lohse
+1	1.8616174	-3.545	3.22	0.2128	$\chi_{PT}$
$\mu(s)$	1.8614390	-3.367	3.37	0.2031	$\chi_{PT}$
<i>Predictions from experimental analysis and other models</i>					
	1.858		$2.90_{-2.10}^{+\infty}$		Afanasyev [20]
	1.865	-7.0	3.20		Efimov [21]



TABLE V.  $K^+N$   $s$ -wave scattering lengths from several models and experiment.

Modell	$a_0 (T = 0)$ [fm]	$a_0 (T = 1)$ [fm]	Ref.
SP92	0.00	-0.33	[6]
Inversion	0.00	-0.33	
Meson Ex. (A)	0.03	-0.26	[27]
Meson Ex. (B1)	-0.15	-0.32	[27]

TABLE VI.  $K\pi$   $s$ -wave scattering lengths from different theoretical models and experimental analyses.

Model	$a_0^1 [m_\pi^{-1}]$	$a_0^3 [m_\pi^{-1}]$	Ref.
Estabrooks	0.331	-0.138	[8]
Inversion	0.340	-0.147	
Meson Ex.	0.23	-0.064	[18]
$\chi$ PT	0.17	-0.05	[28]
Quark model	0.23	-0.077	[29,30]

TABLE VII.  $K\bar{K}$  isoscalar scattering lengths from [9] and their reproduction by inversion potentials.

Modell	Re $a_K$ [fm]	$R_K$ [fm]	$V_K$ [fm <sup>3</sup> ]
Set 1	-1.73	0.38	-0.66
Inversion	-1.73	0.38	
Set 2	-1.58	0.20	-0.83
Inversion	-1.58	0.20	

TABLE VIII. Yukawa parameters. The mass of the exchanged particle is given by  $\mu = \frac{mc}{\hbar}$ .

	$Y$ [MeVfm]	$\mu$ [fm <sup>-1</sup> ]	$m$ [MeV]
$pp$	14.4	0.684	134.97
$K^+N$	1325.85	2.9436	580.85
$K\bar{K}$	1923.59	1.316	259.68
$\pi N$	111.84	1.61	317.70
$\pi K$	638.1	1.87	368.4
$\pi\pi$	1081.28	2.219	437.87

## FIGURES

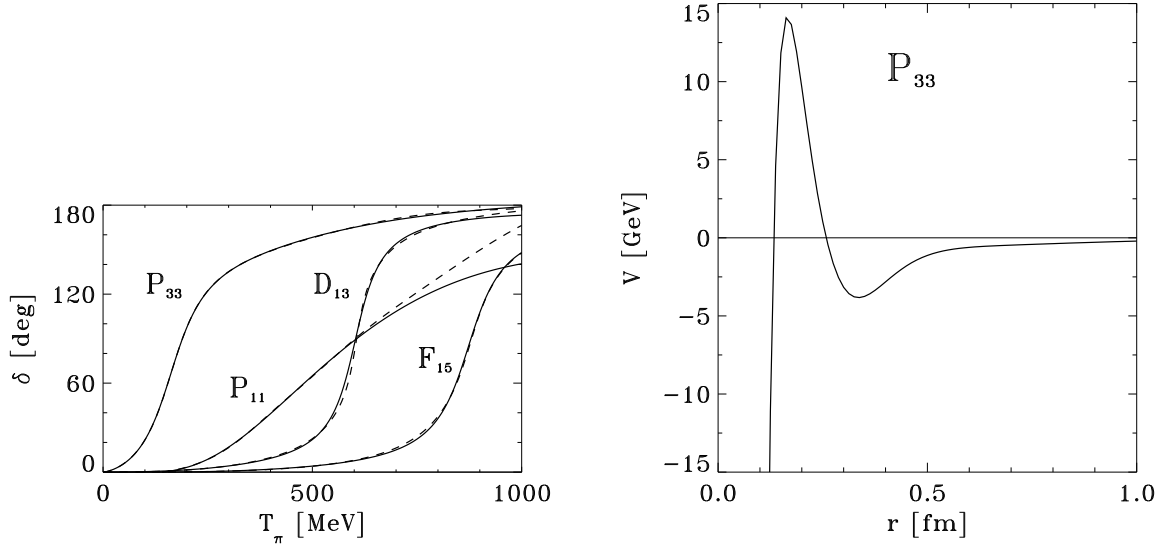


FIG. 1. Left:  $\pi N$  real phase shifts in the resonant channels (dashed) and their reproduction by the inversion potentials (full line). Right:  $\pi N$   $P_{33}$  potential from quantum inversion.

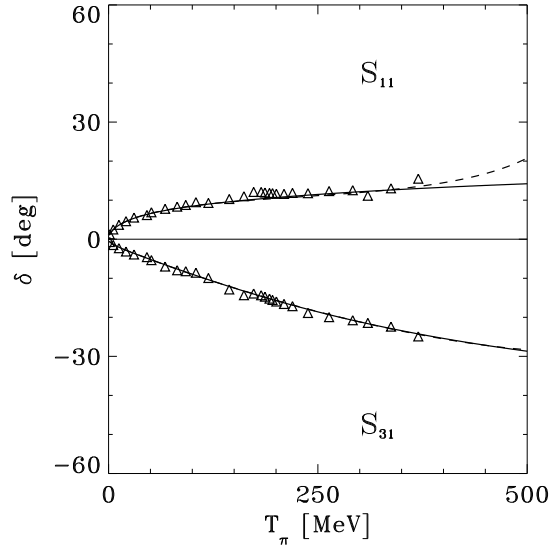


FIG. 2.  $\pi N$  SM95 [5] (dashed line) and KH80 [12] (triangles) data with reproduction by inversion potentials (solid line) for the  $\pi N$   $S_{11}$  and  $S_{31}$  channels.

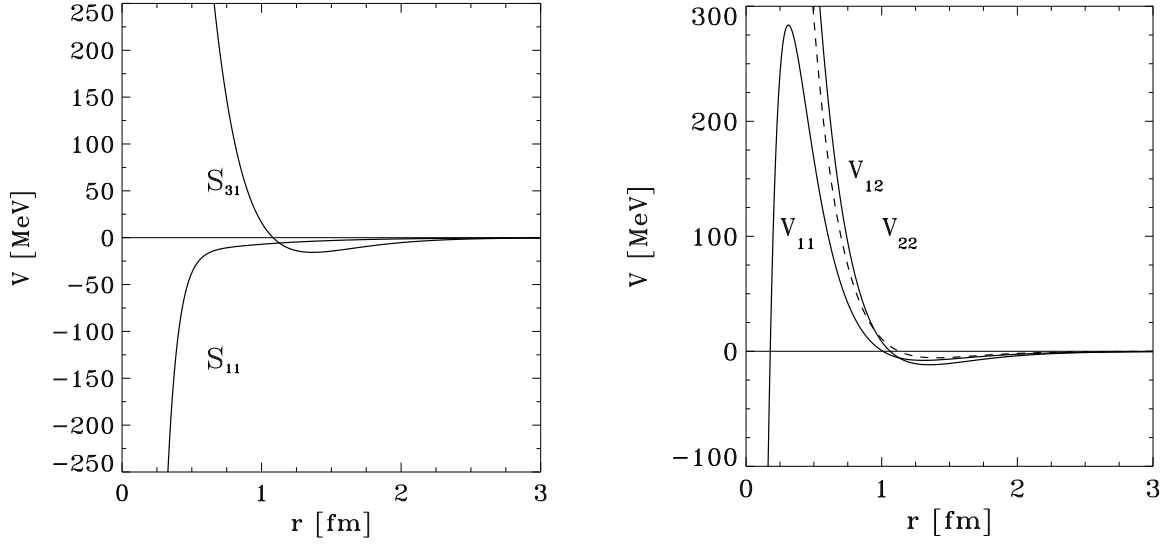


FIG. 3.  $\pi N$  inversion potentials using SM95 phase shifts (left), and the potential matrix (right).

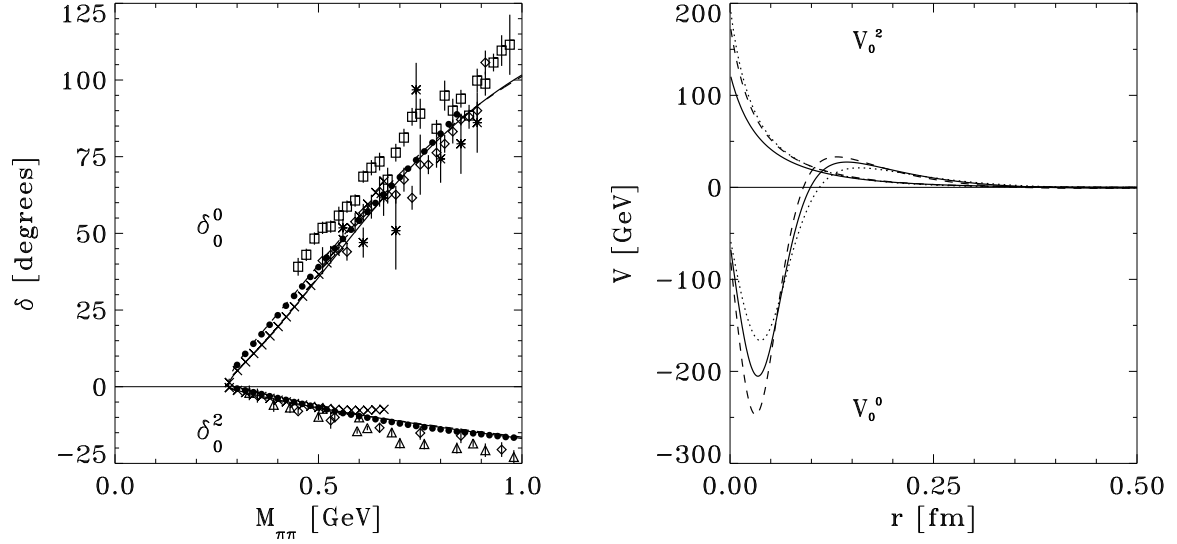


FIG. 4. Left:  $\pi\pi$   $\ell = 0$  phase shifts from  $\chi$ PT (crosses) and the reproduction by the inversion potentials (full line), from the analysis by Froggatt (dots) and the reproduction by the inversion potentials (dashed). Right:  $\pi\pi$   $\ell = 0$  inversion potentials based on phase shifts from  $\chi$ PT (full line), the analysis by Froggatt (dashed) and meson exchange (dotted).

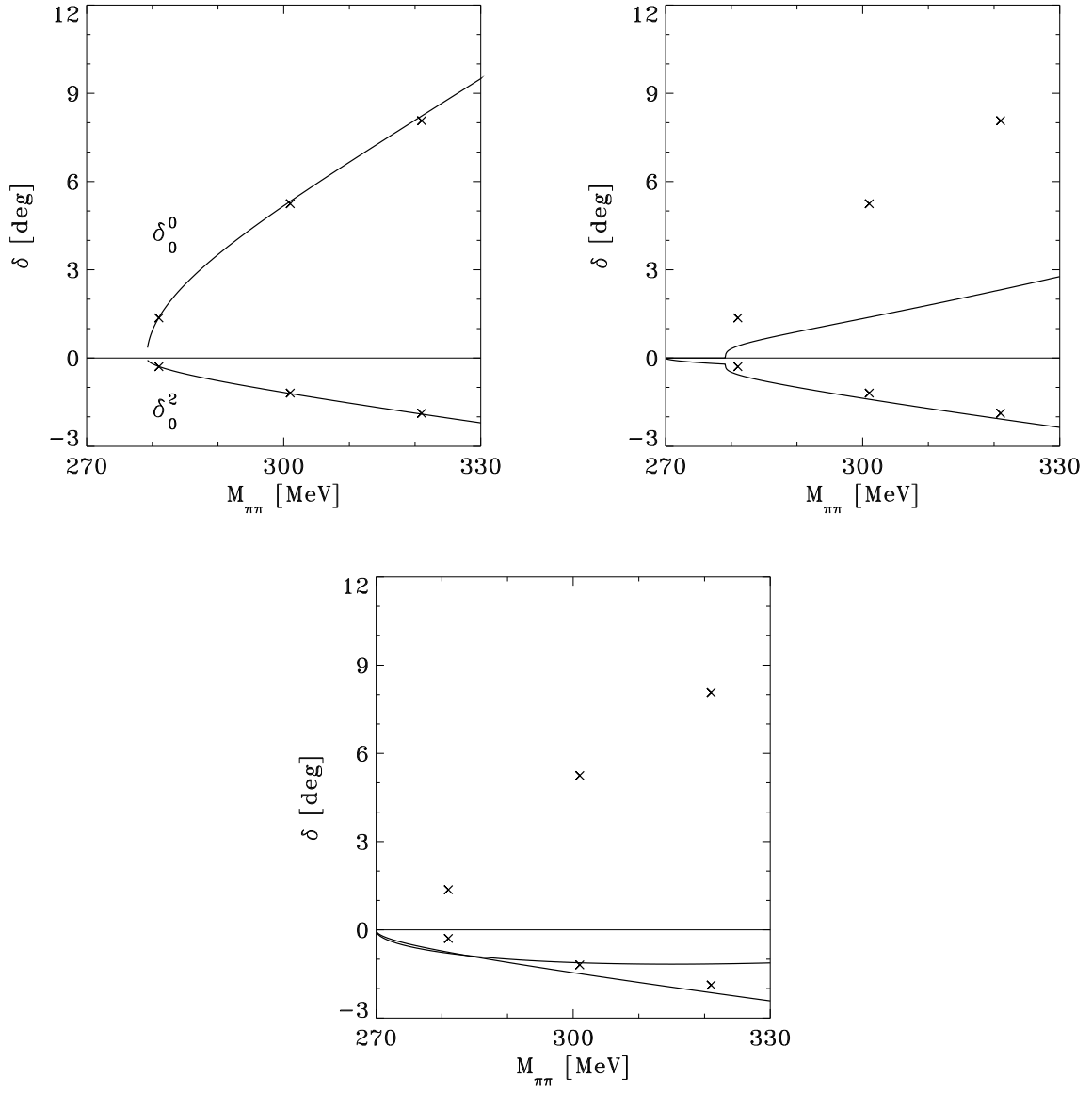


FIG. 5. Eigenchannel phase shifts. More details given in the text.

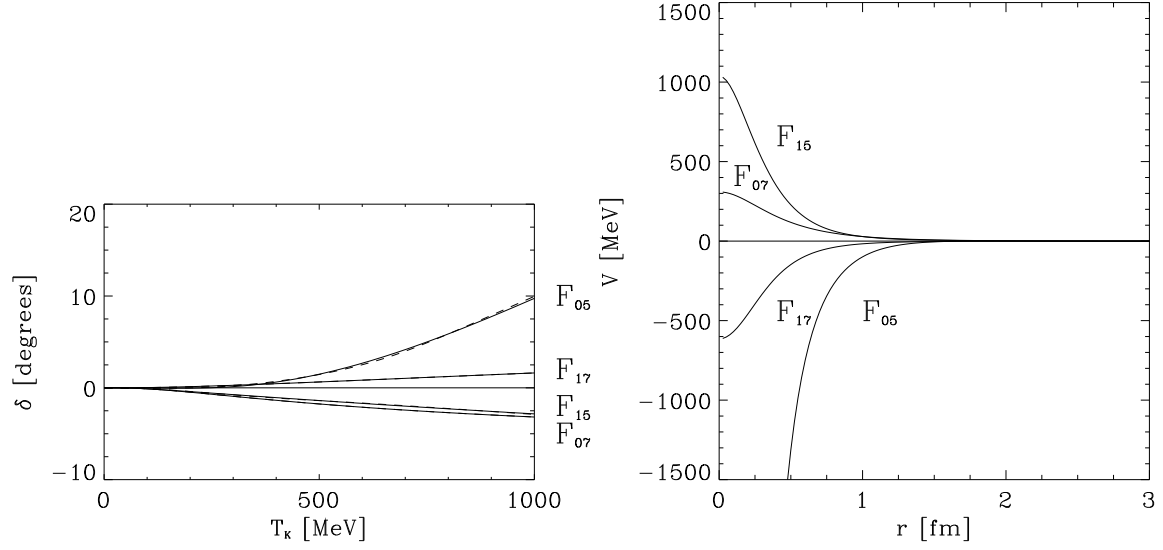


FIG. 6. Left:  $K^+N$   $\ell = 3$  phase shifts from the analysis SP92 [6] (dashed) and their reproduction by the respective inversion potentials (full line). Right:  $K^+N$   $\ell = 3$  inversion potentials.

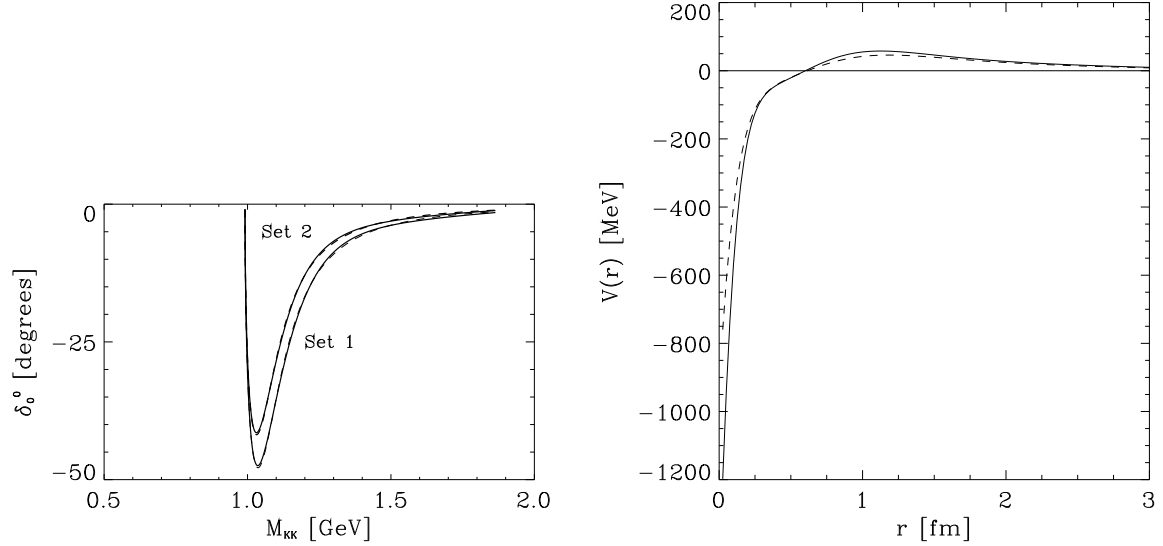


FIG. 7. Left:  $K\bar{K}$   $\ell = 0$  real isoscalar phase shifts calculated from the effective range expansion (dashed) using the parameters given by Kaminski and Lesniak [9] and their reproduction by the inversion potentials (full line). Right:  $K\bar{K}$   $\ell = 0$  real isoscalar potentials from quantum inversion based on the two sets of parameters given by Kaminski and Lesniak [9], set 1: full line, set 2: dashed.